Measuring and Modeling the Primary Organic Aerosol Volatility from a Modern Non-Road Diesel Engine

Shantanu H. Jathar[1], Naman Sharma[1], Abril Galang[1], Cody Vanderheyden[1], Manpreet Takhar[2], Arthur W. H. Chan[2], Jeffrey R. Pierce[3], and John Volckens[1]
[1]Department of Mechanical Engineering, Colorado State University, Fort Collins, CO, USA
[2]Department of Chemical Engineering and Applied Chemistry, University of Toronto, Toronto, ON, Canada
[3]Department of Atmospheric Sciences, Colorado State University, Fort Collins, CO, USA
Correspondence to: Shantanu H. Jathar (shantanu.jathar@colostate.edu)

Abstract

Primary organic aerosol (POA) in diesel exhaust is semi-volatile and partitions mass between the gas and particle phases. POA volatility is not well understood for alternative fuels, varying engine loads, and for engines that feature modern emissions controls. In this study, we performed filter-based measurements of diesel exhaust from a modern-day non-road diesel engine for two different fuels (conventional diesel and soy-based biodiesel), two different engine loads (idle and 50% load), and with and without an emissions control device. Filters were analyzed offline to determine the POA volatility in two different ways: positive artifact on quartz filters at varying dilution ratios and speciation of alkanes. The POA volatility determined from our data suggests that POA mass emissions from diesel exhaust may be reduced by a factor of five with dilution to atmospherically relevant concentrations. These results are generally consistent with previous literature on POA volatility from non-road diesel engines but not with that from on-road diesel vehicles. POA volatility may hence need to be treated separately for non- and on-road sources in atmospheric models. Surprisingly, the POA volatility did not appear to vary under different combinations of fuel, engine load, and emissions control experiments performed, suggesting that POA might be dominated by unburned lubricating oil and its oxidation products. The POA volatility estimated from the speciation of alkanes was found to agree well with that determined from the dilution experiments. A kinetic model was used to calculate the gas/particle partitioning of POA in the dilution system. The modeling suggests that residence times in the dilution tunnel need to be on the order of minutes to allow the POA in the diluted exhaust to achieve gas/particle equilibrium. The use of short residence times (less than tens of seconds), similar to those used in conventional dilution systems, may bias the measurement of POA mass emissions in such systems and is of particular concern for emissions from cleaner, more modern combustion sources. The precise magnitude and direction of the bias depends on the exhaust temperature before dilution, tailpipe seed concentrations, dilution ratio, and residence times in the dilution tunnel. We recommend that kinetic models such as those used in this work be used, instead of using equilibrium assumptions, to inform the design and operation of the dilution tunnels as well to interpret the POA volatility from measurements made with those dilution tunnels.

Abbreviations

BC - Black carbon
DOC - Diesel oxidation catalyst
DPF - Diesel particulate filter
EC - Elemental carbon
OC - Organic carbon
OM - Organic matter
$PM_{2.5}$ - Particulate Matter smaller than 2.5 µm

POA - Primary Organic Aerosol

Keywords
primary organic aerosol; volatility; combustion emissions; gas chromatography; gas/particle partitioning; kinetic modeling

1. Background

Combustion sources such as motor vehicles, electricity generating units, cookstoves, and wildfires emit fine particles or particulate matter smaller than 2.5 microns ($PM_{2.5}$) as a result of incomplete combustion. $PM_{2.5}$ is an important atmospheric pollutant that has large yet uncertain impacts on climate (Pachauri et al., 2014) and adversely affects air quality (Fuzzi et al., 2015) and human health (Pope et al., 2009). Diesel engines and vehicles are important sources of $PM_{2.5}$ at local and regional scales and account for about three-quarters of the $PM_{2.5}$ contributed by mobile sources in the United States (Dallmann and Harley, 2010) and even more so globally (Anenberg et al., 2019). Diesel $PM_{2.5}$ is primarily composed of black/elemental carbon (BC/EC) and primary organic aerosol (POA), with minor contributions from inorganic compounds and metals (Cheung et al., 2010; Schauer et al., 1999). While BC/EC is widely believed to be non-volatile in the atmosphere, diesel POA is known to be semi-volatile, i.e., the organic compounds that constitute POA partition their mass between the gas and particle phases (May et al., 2013a,b,c; Robinson et al., 2007). Dilution from atmospheric mixing and variations in ambient temperature are hence expected to alter the gas/particle partitioning of POA and control the fate, lifetime, and impacts of atmospheric POA.

The volatility of POA from diesel exhaust, in addition to that from gasoline exhaust (May et al., 2013b), biomass burning (May et al., 2013a), and food cooking (Mohr et al., 2009); (Huffman et al., 2009), has been extensively studied. Lipsky and Robinson (2006) and Robinson et al. (2007) used a small diesel generator and an isothermal dilution system to study the change in POA mass emissions with dilution. Both studies found dilution to atmospherically relevant concentrations (~10 $\mu g\ m^{-3}$) resulted in ~80% of the tailpipe diesel POA mass to evaporate. Building on this initial work, the same diesel generator was used in two follow-up studies. Grieshop et al. (2009) used a thermal denuder to constrain the gas/particle partitioning of diesel exhaust POA at even lower atmospheric concentrations of POA (<10 $\mu g\ m^{-3}$) while Ranjan et al. (2012) used an environmental chamber instead of a dilution system. Both studies validated findings from the earlier work. May et al. (2013c) investigated the gas/particle partitioning of POA emissions from two medium-duty trucks, three heavy-duty trucks, and one transportation refrigeration unit using four independent but complementary methods: positive artifacts on quartz filters, dilution to an environmental chamber, heating with a thermal denuder, and POA speciation using gas chromatography mass spectrometry. They found that these real-world POA mass emissions were less volatile than that from the small diesel generator and 20% of the POA mass was possibly non-volatile. Li et al. (2016) measured the gas/particle partitioning of POA emitted by a mixture of gasoline and diesel vehicles in a traffic tunnel in Pittsburgh, PA and observed that the partitioning of ambient POA was qualitatively similar to the partitioning observed with POA from source/laboratory testing of gasoline and diesel vehicles. This result suggested that laboratory parameterizations could be directly used to model POA gas/particle partitioning in atmospheric models. Although it is clear that diesel exhaust POA is semi-volatile, prior work has mostly focused on emissions from a small generator at a specified load and averaged emissions

over a vehicle drive cycle. There are few data on diesel engine operation across engine loads that might be more relevant for non-road engines that operate at steady-state loads (Guan et al., 2017). Further, with wider adoption of alternative fuels (e.g., biodiesel) and the requirement of emissions control systems to meet current emissions standards, there is a need to investigate the semi-volatile behavior of POA from diesel engines with changes in fuel and addition of emissions control systems.

Some prior work has used isothermal dilution performed with dilution tunnels in conjunction with quartz filter measurements to estimate the volatility of POA arising from combustion sources (Grieshop et al., 2009; May et al., 2013b,c; Robinson et al., 2007). Isothermal dilution is an appropriate method to assess POA volatility since it is expected to closely mimic the physical process of diluting source emissions into the atmosphere. In these studies, the POA volatility was interpreted and parameterized by examining the positive artifact measured on simultaneously collected quartz and quartz-behind-Teflon filters, over a range of dilution ratios (Subramanian et al., 2004). In performing filter measurements, earlier work has assumed that the particles have been collected onto filters after the POA has achieved equilibrium between the vapor and particle phases. However, if equilibrium is not achieved, the fraction of the organic matter collected on the bare quartz and quartz behind Teflon filters will vary and alter the POA volatility interpreted through an analysis of the positive artifact. For instance, an excess in the vapor phase would increase the relative magnitude of the positive artifact and suggest a more volatile POA when compared to that at equilibrium. This effect is unlikely to be very sensitive to the amount of time sampled onto the filter. Excess POA in the vapor or particle phases could also bias POA measurements made with direct reading instruments (e.g., aerosol mass spectrometer) such as those used by Ranjan et al. (2012) and Kuwayama et al. (2015) to measure POA volatility. Lipsky and Robinson (2006) performed isothermal dilution experiments on emissions from a small diesel generator at varying residence times (2.5 and 40 s) and found that the POA mass measurements were nearly identical between the two residence times, indicating that equilibrium was achieved over short timescales (<2.5 s). However, the small diesel generator they used produced very high $PM_{2.5}$ emissions (1.5-4 g kg-fuel^{-1}), which meant that the particle surface area even at high dilution ratios was sufficient (>0.01 m^2 m^{-3}) to ensure large condensational sinks and short equilibration timescales (<2 s). Modern sources, such as super ultra-low emissions vehicles or vehicles equipped with diesel particulate filters, have significantly lower $PM_{2.5}$ emissions (median of ~0.008 (Saliba et al., 2017) and ~0.003 g kg-fuel^{-1} (May et al., 2014), respectively), and hence the condensational sinks might be too small (<10^{-3} m^2 m^{-3}) and the equilibration timescales might be too large (>30 s) after dilution to assume equilibrium in conventional dilution systems (e.g., constant volume samplers) where residence times are typically less than ten seconds (40 CFR §1065, 2005) (Kim et al., 2016). Further, Riipinen et al. (2010) showed that equilibrium assumptions should not be used to estimate POA volatility when using thermal denuder systems (heating, rather than dilution) but rather rely on kinetic models for accurate estimates. It seems that there is a need to apply models that simulate the kinetic condensation/evaporation of POA in sampling and dilution systems to test assumptions about POA equilibrium prior to measurement and assessing their influence on parameterizing the POA volatility for atmospheric models.

More recently, thermal desorption gas chromatography mass spectrometry (Presto et al., 2012, 2010; Zhao et al., 2016, 2015, 2014; Worton et al., 2014) and chemical ionization mass

spectrometry performed via a filter inlet for gas and aerosol (Lopez-Hilfiker et al., 2016, 2014; Stark et al., 2017) have been used to infer organic aerosol volatility. The TD-GC/MS technique uses the retention time through the GC column while the FIGAERO-CIMS technique uses the response to a temperature ramp to map the measured organic compounds to a specific volatility. May et al. (2013b,c) showed that the volatility of gasoline and diesel exhaust POA estimated from the TD-GC/MS reasonably matched the volatility estimated through the positive artifact on quartz filters. Since these techniques allow for estimation of the volatility from a single sample, they are better suited than dilution-based studies to characterize organic aerosol volatility in source and ambient samples and track changes in volatility with time. However, to our knowledge, the volatility distributions estimated from the TD-GC/MS or FIGAERO-CIMS data have not been compared against volatility distributions estimated from isothermal dilution data. These techniques need to be validated before they are widely used to quantify organic aerosol volatility.

In this work, we measured and modeled the volatility of POA from a modern-day diesel engine under varying fuel, engine load, and emissions control configurations. The POA volatility was investigated using two independent techniques: positive artifacts on quartz filters and distribution of alkanes inferred via TD-GC/MS. The gas/particle partitioning behavior of POA during the sampling and dilution process was simulated using a kinetic condensation/evaporation model.

2. Methods

2.1 Experimental Methods

Engine Experiments and Setup. We used a 4-cylinder, turbocharged and intercooled, 4.5 L, 175 hp, John Deere 4045H PowerTech Plus engine, mounted on an engine dynamometer (Midwest Inductor Dynamometer 1014A). The stock engine met the Tier 3 emissions standards for non-road engines. An emissions control system consisting of a diesel oxidation catalyst (DOC) and a diesel particulate filter (DPF) was retrofitted on the exhaust system to meet non-road interim Tier 4 emissions standards (40 CFR §1039, 2004) but the engine was not recalibrated to optimize performance and emissions. This engine has been used extensively in the past for studies ranging from quantifying the influence of alternative fuels on tailpipe emissions to studying the ability of diesel exhaust particles to form ice nuclei (Drenth et al., 2014; Schill et al., 2016). A companion paper studied the oxidative reactivity of diesel exhaust particles using a dithiothreitol chemical assay (Sharma et al., 2019).

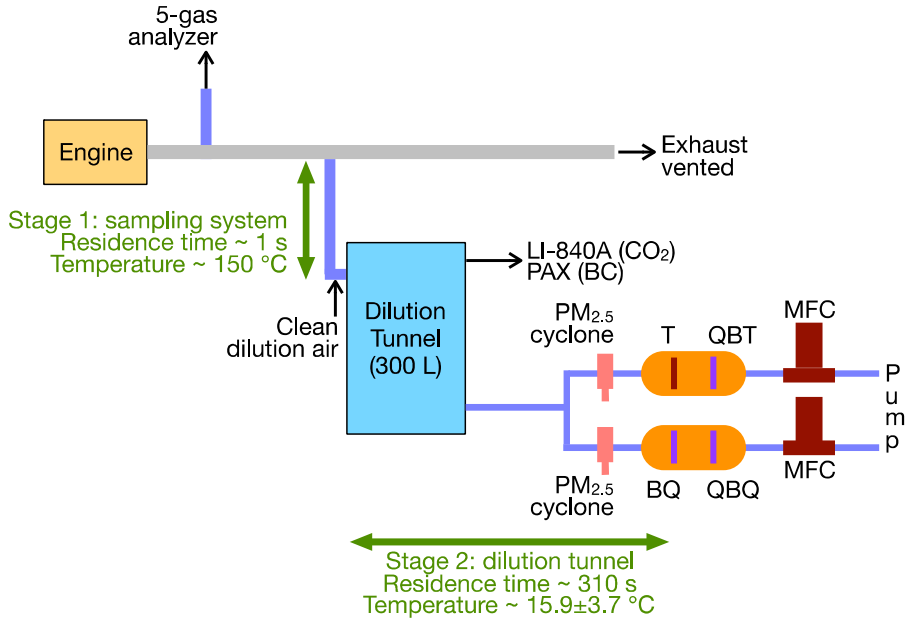

Figure 1: Schematic visualizing the experimental setup, particle collection, and the two stages used to model gas/particle partitioning of POA. T = Teflon filter, QBT = Quartz Behind Teflon filter, BQ = Bare Quartz filter, QBQ = Quartz Behind Quartz filter, MFC = mass flow controller.

Emissions from the tailpipe were sampled through an isokinetic probe and 4.6 m of Silcosteel® tubing heated to 150 °C into a Hildemann-style dilution tunnel using activated charcoal- and HEPA-filtered clean air (Hildemann et al., 1989). A schematic of the sampling setup is shown in Figure 1. The chemical passivation of the inside tube walls using SilcoNert® 1000 and heating of the tube outer surface were done to prevent loss of semi-volatile organic compounds to the tube walls - key to preserving the integrity and estimating the POA volatility. The amount of clean air mixed with the exhaust (aka dilution air) was varied using a needle valve that throttled the suction on the pump used to run the dilution tunnel. This method produced varying dilution ratios (ratio of clean air to exhaust), ranging from slightly under 4 to up to 400. For each experiment, the dilution ratio was varied between four to seven steps to produce different absolute concentrations of the pollutants. The dilution ratio range was smaller in case of the emissions control experiments as the tailpipe concentrations were substantially lower than in the absence of an emissions control. A fraction of the diluted exhaust was diverted to the top of a 300 L stainless steel residence tank, which was then used as a reservoir to sample the diluted diesel exhaust. The flow rates in the residence tank were such that the diluted exhaust had a residence time of approximately 310 s, which was sufficient to achieve thermal equilibrium. Assumptions about thermodynamic equilibrium were tested with a kinetic condensation/evaporation model, discussed later. The influence of particle and vapor loss to the walls of the residence tank was minimized by sampling from the bottom-center of the tank.

The engine was operated in different fuel, engine-load, and emissions-control combinations. Two different fuels were used: (i) non-road, red dyed, diesel sourced from Team Petroleum (Fort Collins, CO) and (ii) soy-based biodiesel sourced from Emergent Green Energy (Minneola, KS). The engine was run at two different loads: (i) idle conditions that corresponded to a 0% load (0

kW at 900 rpm) and (ii) load conditions that corresponded to 50% load (60 kW at 2200 rpm). The engine was operated with and without the emissions control system that consisted of the DOC (that oxidized unburned hydrocarbons and CO) and DPF (that filtered fine particles). We performed measurements at multiple dilution ratios for each combination of fuel, engine load, and emissions control. The experimental matrix that included 65 total experiments is listed in Table 1.

Table 1: List of the fuel-engine load-emissions control experiments performed in this work and dilution ratio details.

Fuel-Load-Emissions Control	***# of Experiment Days***	***Dilution Ratio Range***	***Number of Unique Dilution Ratio Experiments***
Diesel-Idle-None (Tier 3)	3	3-468	19
Diesel-Load-None (Tier 3)	3	4-222	11
Biodiesel-Idle-None (Tier 3)	3	3-200	16
Biodiesel-Load-None (Tier 3)	3	3-127	10
Diesel-Idle-DPF+DOC (Tier 4)	1	3-107	4
Diesel-Load-DPF+DOC (Tier 4)	2	2-8	5

Emissions Measurements. Tailpipe emissions from the diesel engine were transferred through a Teflon® line heated to 110 °C to a 5-gas analyzer (Siemens, Germany) to measure raw concentrations of CO_2, CO, O_2, THC (total hydrocarbons), NO, and NO_2. Carbon dioxide concentrations of the diluted exhaust in the residence tank were measured using a LI-840A (LI-COR Environmental, Nebraska). This allowed for the calculation of the dilution ratio as follows: (Lipsky and Robinson, 2006)

$$Dilution\ Ratio\ (DR) = \frac{CO_2|_{undiluted} - CO_2|_{background}}{CO_2|_{diluted} - CO_2|_{background}} \quad (1)$$

where undiluted, diluted, and background concentrations were those measured in the tailpipe, residence tank, and the dilution air respectively. A photoacoustic extinctiometer (PAX) (Droplet Measurement Technologies, Colorado), connected to the residence tank, was used to measure BC mass concentrations (Lack et al., 2006).

Diluted emissions in the residence tank were drawn at 16.7 L min^{-1} through a $PM_{2.5}$ cyclone (URG Corp., North Carolina) followed by a custom-built filter cartridge that hosted two filters in series. Two filter cartridges were connected in parallel to collect $PM_{2.5}$ in the following manner. The first cartridge contained a front Teflon® filter to collect particles only and a quartz filter behind it to trap semi-volatile vapors (hereafter referred to as the quartz behind Teflon® or QBT filter). The second filter cartridge contained a front quartz filter to collect all particles and trap semi-volatile vapors (hereafter referred to as the bare quartz or BQ filter) and a quartz filter behind it to only trap semi-volatile vapors (hereafter referred to as quartz behind the quartz or QBQ filter). The hydrophobic Teflon® filter is expected to minimize the adsorption of semi-volatile vapors while the quartz filter has been shown to collect semi-volatile vapors with a saturation concentration up to 10^4 µg m^{-3} (May et al., 2013a,b,c). In addition to sampling $PM_{2.5}$, we performed a set of dynamic blank experiments to account for semi-volatile vapors present in the dilution air, and we performed a set of handling blank experiments to account for artifacts introduced through filter handling and storage. We conducted a total of 10 dynamic blank

experiments and 6 handling blank experiments, which accounted for 20% of all data collected. All filters were 47 mm in size, with the Whatman Teflon® filters (7592-104) sourced from GE Healthcare Life Sciences (UK) and the Pallflex quartz filters (2500 QAT-UP) sourced from Pall Corporation (New York). Details of the filter cartridge setup can be visualized in Figure 1 and details about the filter preparation, handling, and storage are described in the SI in Section S1.

$PM_{2.5}$ Mass and Composition Measurements. A gravimetric measurement was performed with an MX5 microbalance (Mettler Toledo, Switzerland) to determine the $PM_{2.5}$ mass collected on all Teflon® filters. The organic and elemental carbon (OC and EC) mass on all BQ and QBT filters was measured using a semi-continuous version of the Sunset Model-4 OC/EC analyzer (Sunset Laboratory Inc., Oregon) following the NIOSH 5040 method (Eller and Cassinelli, 1996). POA was determined by multiplying the OC with an organic-matter-to-organic-carbon ratio of 1.2 (May et al., 2013c; Turpin and Lim, 2001). BC mass collected on all Teflon® filters was optically measured using the SootScan Model OT21 Optical Transmissometer (Magee Scientific, California). $PM_{2.5}$, POA, EC, and BC mass concentrations were calculated by knowing the total mass on the filter and the total volume of air (at standard temperature and pressure) sampled and recorded by the mass flow controller. All $PM_{2.5}$, POA, EC, and BC measurements were corrected for handling and dynamic blanks. More details on each of these measurements can be found in the SI (Sections S2, S3, and S4).

A few select BQ filters were also analyzed using TD-GC/MS to speciate the $PM_{2.5}$ mass. Filters 4 mm in diameter were punched, put into glass tubes (6 mm OD × 7" length, Gerstel), and loaded into a thermal desorption system (TDS; Gerstel GmbH, Germany). A maximum of four filter punches per analysis were run in the TDS. To desorb the organic compounds from the filter punches, the temperature in the TDS was ramped from an initial temperature of 40 °C to 320 °C at a ramp of 60 °C min^{-1} and then held for 5 minutes at 320 °C. Once desorbed, the organic compounds were carried in a helium flow to a cooling injection system (CIS4; Gerstel GmbH, Germany) via a transfer line maintained at 320 °C. The CIS4 was embedded with a quartz wool filled quartz liner maintained at an initial temperature of 20 °C during thermal desorption to focus the desorbed compounds from the TDS. After 30 min, the CIS4 was then heated to 320 °C at a ramp of 12 °C s^{-1} and held for 10 minutes to transfer the analytes to the GC column. During the analysis, the GC oven was heated from 50 °C to 300 °C using a ramp of 10 °C min^{-1} and held for an additional 5 minutes at 300 °C. The GC column used was a non-polar 30 m × 0.25 mm ID × 0.25 µm column (Rxi-5ms, Restek, Pennsylvania). *N*-alkanes were quantified based on authentic standards. All alkanes (including *n*-alkanes) were quantified using the signal at m/z 57 based on the method by Zhao et al. (2015) (explained in Section 2.2). Fatty acid methyl esters were also observed for the biodiesel samples and they were quantified using the signal at *m/z* 74 (Oliviera et al., 2008; Pauls et al., 2011).

2.2 Data Analysis

Emission Factors. Emission factors for the gas- (CO_2, CO, NO_X, THC) and particle-phase ($PM_{2.5}$, POA, EC, inorganic ions, metals) pollutants were calculated to compare emissions at different fuel, engine-load, and emissions-control combinations and to facilitate comparison with values in the literature. The emission factors in units of g kg-$fuel^{-1}$ were calculated as follows:

$$EF_X = \frac{\Delta X}{\Delta CO_2} \times \frac{MW_{CO_2}}{AW_C} \times C_f \times 10^3 \quad (2)$$

Where ΔX and ΔCO_2 are the background-corrected pollutant and CO_2 concentrations in µg m^{-3} respectively, MW_{CO_2} (44 g mole^{-1}) and AW_C (12 g mole^{-1}) are the molecular/atomic weights for CO_2 and carbon, and C_f is the mass fraction of carbon in the fuel. According to Gordon et al. (2014), we used a C_f of 0.85 g kg-fuel^{-1} for diesel and 0.77 g kg-fuel^{-1} for biodiesel. This formulation for the emission factor calculation assumes that all of the carbon in the fuel was released as CO_2.

POA Volatility. The POA volatility was assessed using two different methods: positive artifact on quartz filters and alkane speciation using the TD-GC/MS. In the first method, we used the positive artifact from vapor adsorption on the BQ and QBT filters to calculate the fraction of POA in the particle phase (X_p). This technique has been used extensively in the past to quantify POA volatility (Robinson et al., 2007; Shrivastava et al., 2006) and was recently validated for diesel exhaust POA against three independent techniques (May et al., 2013c). Following May et al. (2013c), X_p was calculated as follows:

$$X_p = \frac{OC_{BQ} - OC_{QBT}}{OC_{BQ}} \quad (3)$$

Where OC_{BQ} and OC_{QBT} are the OC mass concentrations in units of µg C m^{-3} on the BQ and QBT filters respectively. Typically, X_p is plotted against the POA mass concentration to visualize changes in the gas/particle partitioning with dilution. The gas/particle partitioning behavior was used to determine a volatility distribution for POA that reflected the distribution of vapor pressures of the organic compounds that constitute POA. This volatility distribution can be described with the volatility basis set (VBS) framework using a set of semi-volatile surrogate species that are logarithmically spaced in volatility or saturation concentration space (Donahue et al., 2006). The following equation describes the gas/particle partitioning of POA:

$$X_p = \Sigma\, f_i \left(1 + \frac{C_i^*}{POA}\right)^{-1} \quad (4)$$

Where f_i is the fraction of the total (gas+particle) mass in bin *i* and C_i^* is the effective saturation concentration for bin *i* in µg m^{-3} at 298 K. For a predefined C^* set of [10^0 10^1 10^2 10^3 10^4 10^5] µg m^{-3}, the gas/particle partitioning data were fit to determine an f_i set that represented the POA volatility distribution. The method assumes that the POA was in equilibrium before it was sampled onto the filters. This assumption will be tested and discussed as part of the kinetic modeling sections described later.

In the second method, the distribution of linear alkanes and all alkanes determined from the TD-GC/MS analysis was mapped in VBS space, similar to the approach used by Zhao et al. (2016, 2015, 2014). Briefly, the chromatogram was divided into retention time bins, and the average volatility of each bin was inferred from *n*-alkane retention times. Since the GC column used a non-polar stationary phase, retention times of aliphatic compounds corresponded to their boiling points and, consequently, vapor pressures. The vapor pressures for the *n*-alkanes were calculated using the group contribution method of SIMPOL.1 (Pankow and Asher, 2008). The signal of the *m/z* 57 ion was used to infer the mass in each volatility bin since this ion corresponds to MS fragments from aliphatic species (paraffins, olefins, and naphthenes). "Linear alkanes" were calibrated using a suite of authentic *n*-alkane standards to obtain the corresponding mass. For "all alkanes", the total area for the signal at *m/z* 57 in each bin was converted to mass using the response factors of *m/z* 57 from *n*-alkane standards. This is based on the same assumption made by Zhao et al. (2015) that "all alkanes" have an average response factor similar to that of *n*-alkanes of similar volatility. FAMEs were explicitly measured in all samples using the signal at

m/z 74 but we only used the signal at m/z 57 to construct the volatility distribution for the biodiesel samples since the FAMEs were found to be a factor of 5 lower than all alkanes (see Figure S1). The volatility distribution, so produced, was normalized before being used with equation (4) to calculate X_p over a POA mass concentration range.

2.3 Kinetic Modeling of POA Partitioning

We modeled the kinetic gas/particle partitioning of the POA species by solving the mass balance from condensation and evaporation for a polydisperse particle size distribution. We used fifteen logarithmically spaced size bins ranging from 10 to 1000 nm. The following differential equations represent the evolution of the mass concentrations of the POA species in µg m^{-3} in the gas (C_i^g) and particle ($C_{i,j}^p$) phases:

$$\frac{dC_i^g}{dt} = -\sum_j 2\pi D_i^g D_j^p N_j^p F_{FS}\left(C_i^g - \frac{C_{i,j}^p}{COA_j} C_i^* K_j\right) \quad \text{- (5)}$$

$$\frac{dC_{i,j}^p}{dt} = 2\pi D_i^g D_j^p N_j^p F_{FS}\left(C_i^g - \frac{C_{i,j}^p}{COA_j} C_i^* K_j\right) \quad \text{- (6)}$$

Where D_i^g is the gas-phase diffusion coefficient of the partitioning species i in m^2 s^{-1}, D_j^p is the diameter of the particle in size bin j in m, N_j^p is the particle number concentration in size bin j in m^{-3}, $F_{FS}$is the Fuchs-Sutugin correction (see Section S5 in SI), COA_j is the total POA mass concentration in size bin j in µg m^{-3}, C_i^* is the effective saturation concentration of the partitioning species i in µg m^{-3}, and K_j is the Kelvin ratio. We did not model coagulation and nucleation and hence the particle number concentration in each size bin was conserved. The diameter of the particle in size bin j was updated by considering the mass addition/removal of POA to the initial seed mass. Finally, the Kelvin ratio was approximated using the following equation (Tröstl et al., 2016):

$$K_j = 10^{\frac{3.75\times10^{-9}}{D_j^p}} \quad \text{- (7)}$$

The kinetic gas/particle partitioning of the organic matter (OM) was simulated in two stages: (i) partitioning of the undiluted exhaust in the sampling system (from the sampling point in the tailpipe to before dilution) and (ii) partitioning of the diluted exhaust in the dilution tunnel (from the start of dilution to before filter sampling). Here, we define OM as the sum of the total organic material mass in the particle and vapor phases with the particle phase mass termed POA. We did not model the OM partitioning in the tailpipe because all OM mass was likely to be exclusively in the vapor phase at typical tailpipe temperatures for diesel engines (>300 °C) (Ko et al., 2019). In the sampling system (i.e., stage 1), the undiluted exhaust was assumed to be at 150 °C, where the average residence time was ~1 s for the experiments performed in this work. The model was initialized with EC (acting as seed) and OM mass concentrations that were calculated by multiplying the mass concentrations measured on the BQ filter with the dilution ratio. The OM mass was initialized to be exclusively in the vapor phase (i.e., no mass in the particle phase or no POA). We used a small amount of non-volatile OM mass (0.01 µg m^{-3}) to initiate condensation. No particle size distributions were measured in this work so we used a representative normalized particle size distribution from earlier work involving a non-DPF diesel truck (Ning et al., 2013) (number mean = 85 nm, geometric standard deviation = 1.7) to determine the initial size distribution for EC. We assumed spherical particles and an EC density of 1.8 g cm^{-3} (Zhang et

al., 2016). In the dilution tunnel (i.e., stage 2), the diluted exhaust was assumed to be at 25 °C. The BC and POA were initialized for stage 2 by dividing the model outputs from the stage 1 by the dilution ratio. Both stages were modeled for all the experiments performed in this work.

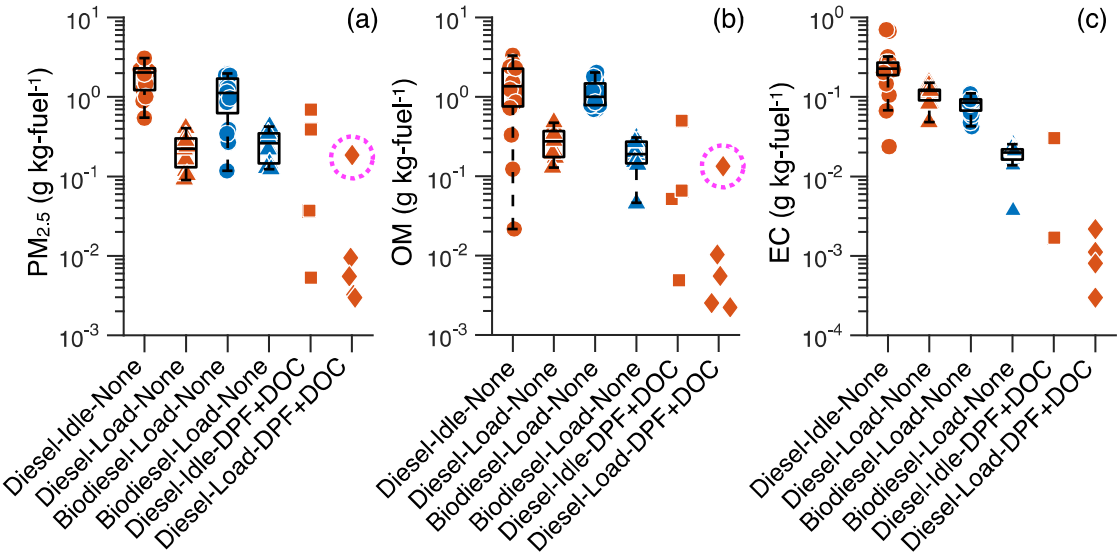

Figure 2: Emission factors of (a) $PM_{2.5}$, (b) OM, and (c) EC in units of g kg-fuel^{-1} for the different fuel, engine-load, and emissions-control combinations measured on the filters at the conclusion of stage 2. Outliers for the DPF+DOC experiments at the 50% load condition, identified visually, are circled in magenta.

3. Results

3.1 Gas and Particle Emissions

Emission factors for the gas-phase species (CO_2, CO, NO_X and THC) were compared across the various fuel, engine-load, and emissions-control combinations (see Figure S2). The comparison is described in detail in SI Section S6, but we briefly mention the key findings here. Compared to diesel, CO_2 emissions from the use of biodiesel were ~10% lower on account of a lower carbon mass fraction in biodiesel. On average, emission factors of CO and THC were higher at the idle condition compared to the 50% load condition from incomplete combustion and lower with the use of biodiesel compared to diesel. In contrast, NO_X emissions were mostly unaffected by fuel, engine load, or emissions control. As seen in a previous study with this engine (Jathar et al., 2017), CO and THC emissions at the idle condition were similar when run with and without emissions control suggesting that the emissions control system may be limited at idle, where the catalyst temperatures might be lower than the light off temperatures for effective oxidation of CO and THC (Sumiya et al., 2009).

In Figure 2, we plot the emission factors for $PM_{2.5}$, OM, and EC for all the data measured in this study. Median emissions of $PM_{2.5}$, OM, and EC were higher at the idle condition when compared to the 50% load condition, from incomplete combustion at lower loads. With the exception of one point (circled in magenta), emissions of $PM_{2.5}$, OM, and EC with the DPF+DOC at the 50% load condition were one to two orders of magnitude lower than without the DPF+DOC. These reductions agree well with previously observed reductions with the use of a DPF, which are

401 expected to reduce particle emissions by 95% or more (Biswas et al., 2009; May et al., 2014). In
402 the one instance at the 50% load condition (circled in magenta) and several instances at the idle
403 condition, $PM_{2.5}$ and OM emissions with the DPF+DOC were similar to those without the
404 DPF+DOC. We suspect that in these cases the OM vapors escaped oxidation in the DOC and
405 nucleated in the dilution tunnel after being cooled (Abdul-Khalek and Kittelson, 1995; Shi and
406 Harrison, 1999). This seemed to happen more often at the idle condition because the catalyst
407 temperatures were low enough to prevent complete oxidation of the OM vapors in the DOC.
408 When compared to diesel, biodiesel use resulted in lower median emissions of $PM_{2.5}$ and OM at
409 the idle condition (43% lower for $PM_{2.5}$ and 33% lower for OM) but had higher emissions at the
410 50% load condition (17% higher for $PM_{2.5}$ and 45% higher for OM). In contrast, with biodiesel
411 use, median EC emissions were 62% lower for the idle condition and 83% lower for the 50%
412 load condition. The lower EC emissions with biodiesel meant that the OM:EC ratios were
413 generally higher for biodiesel compared to diesel. At the 50% load condition, the $PM_{2.5}$, OM, and
414 EC emission factor range for diesel use with and without the emissions control compared
415 modestly with recent emission factors compiled by May et al. (2014) from a range of sources
416 and near-road studies, suggesting that the engine and its operation were representative of in-use
417 engines and engine technology (see Table S1).
418
419 ***3.2 $PM_{2.5}$ Mass Closure and Soot Comparison***
420 To assess mass closure, we compared the sum of the POA and EC mass concentrations measured
421 via the quartz filters against the $PM_{2.5}$ mass concentrations measured via the Teflon filter (Figure
422 S3). The comparison showed significant variability, with 58% and 82% of the data lying within a
423 factor of 2 and 3, respectively. The variability did not appear to correlate with differences in fuel,
424 engine load, or presence of the emissions control. On average, the POA+EC mass concentrations
425 were biased low compared to the $PM_{2.5}$ mass concentrations with a mean normalized bias of 60%
426 and mean normalized error of 87%. This mass closure problem between the Teflon and quartz
427 filters has been seen before for diesel-powered sources without a DPF system (Lipsky and
428 Robinson, 2006; May et al., 2013c; Schauer et al., 2002). For instance, May et al. (2014c) tested
429 three medium and heavy-duty diesel vehicles without a DPF and found that the POA+EC mass
430 concentrations were about half of the $PM_{2.5}$ mass concentrations. The POA+EC mass
431 concentrations were possibly lower than the $PM_{2.5}$ values because we used a low POA:OC ratio
432 (1.2 based on the work of Lipsky and Robinson (Lipsky and Robinson, 2006) and Aiken et al.
433 (Aiken et al., 2008)) and/or we overcorrected for the artifact on the BQ filter. We measured
434 water-soluble ions using Ion Chromatography and metals using Inductively Coupled Plasma
435 Mass Spectrometry on a few select filters and together they accounted for less than 5% of the
436 $PM_{2.5}$ mass and, thus, do not account for the mass closure discrepancy. This mass closure
437 problem needs to be closely investigated in the future.
438
439 We also analyzed the different soot emissions by comparing the two BC and EC mass
440 concentrations against each other (Figure S4). We found that the BC measured by the PAX and
441 SootScan modestly correlated with the EC measured by the Sunset OC/EC (R^2=0.69 for PAX
442 and R^2=0.48 for SootScan), but both measurements of BC were biased low compared to EC,
443 particularly at the higher concentrations. For example, at an EC mass concentration of 100 $\mu g\ m^{-3}$, the PAX BC mass concentration was only 69 $\mu g\ m^{-3}$ and the SootScan BC mass concentration
444 was 45 $\mu g\ m^{-3}$, based on the fits to the data. The EC mass concentrations may be higher than the
445 BC mass concentrations for reasons ranging from protocol-related artifacts in the Sunset OC/EC
446

to assumptions about the mass absorption cross-section used in the PAX and SootScan (Cavalli et al., 2010; Chow et al., 2004).

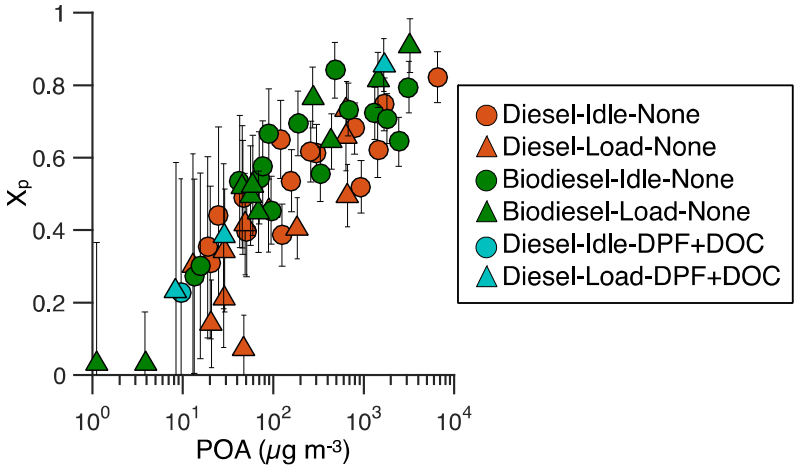

Figure 3: Fraction of POA mass in the particle phase (X_p) plotted against the POA mass concentrations for all experiments performed in this work. The error bars represent the uncertainty in the raw OC/POA measurement made by the Sunset OC/EC analyzer.

3.3 POA Volatility

Changes in the gas/particle partitioning of POA are visualized by plotting the fraction of POA mass in the particle phase (X_p) against the POA mass concentration in Figure 3. Across all experiments, X_p decreased with decreasing POA suggesting that the POA mass evaporated as the POA mass concentration was decreased with increasing dilution. In other words, POA was semi-volatile and was re-partitioning between the gas and particle phases with dilution. Interestingly, we did not observe significant differences in the POA partitioning between the different fuel, engine-load, and emissions-control combinations. Biodiesel POA at both the idle and load conditions appeared to have a slightly lower volatility (or higher X_p) for POA at the higher POA mass concentrations. Overall, the gas/particle partitioning trends implied that while the POA emissions may have varied much more across the different combinations (see Figure 2), the POA volatility was quite similar. One reason why the POA volatility might be similar is that the POA emissions from this engine could have been dominated by unburned or partially burned lubricating oil that was held constant between the different experiments. However, the POA in this work was much more volatile than the volatility measured by Worton et al. (2014) for the unburned lubricating oil used in this work and commonly used in diesel engines (SAE 15W40). Worton et al. (2014) found that ~60% of the lubricating oil mass had a C^* smaller than 10 µg m^{-3} while, as we show below in Figure 4(c), a negligible amount of the POA mass in our work had a C^* smaller than 10 µg m^{-3}. We hypothesize that the POA in our work reflects the more volatile fraction of the lubricating oil that evaporates in the engine cylinder but later condenses in the tailpipe and the dilution tunnel (Worton et al., 2014). This hypothesis needs to be explored in future work.

As the POA volatility did not appear to change with fuel, engine load, or emissions control, data in Figure 3 were used to develop a volatility-distribution fit that represented the POA volatility. The volatility distribution – set of α's as defined in equation (4) – were determined in Matlab

using the non-linear fitting function, 'lsqnonlin'. As the ambient and sample temperatures varied slightly between the different experiments (15.9±3.7 °C) and that the C^*s were predefined at 25 °C or 298 K, we accounted for changes in the C^* with temperature using the Clausius-Clapeyron equation:

$$C^*(T) = C^*(300\ K)\ exp\left(\frac{\Delta H_{vap}}{R}\left(\frac{1}{298} - \frac{1}{T}\right)\right) \text{ - (13)}$$

Where ΔH_{vap} is the enthalpy of vaporization in kJ mole^{-1}, R is the universal gas constant (8.314 kJ mole^{-1} K^{-1}), and T is the temperature in K. The enthalpy of vaporization for use in the Clausius-Clapeyron equation was based on the work of Ranjan et al. (2012):

$$\Delta H_{vap} = -11 log_{10} C^* + 85 \text{ - (14)}$$

The volatility distribution that best fit the data was α=[0.01 0.01 0.2264 0.4 0.0671 0.2008 0.0857] for C^*=[0.1 1 10 100 1000 10000 100000] µg m^{-3} and visualized in Figure 4(c). The values of α sum to 1. The volatility distribution fits were slightly unusual in that they had a small discontinuity in the mass fractions between the C^*=100 and C^*=10,000 µg m^{-3} bins, unlike the smooth volatility distributions inferred from speciation of the POA mass (May et al., 2013c; Worton et al., 2014). The discontinuity in our work is likely to be an artifact of the numerical fitting, although these semi-empirical volatility distributions are unlikely to affect any of the findings from this work.

The POA volatility predicted by the volatility-distribution fits along with the 25th to 75th percentile confidence intervals are compared against the raw measurements in Figure 4(a). The predicted X_p was lower than most of the measurements because the volatility distribution was tied to C^*s predefined at a higher temperature (25 °C) while the POA samples were gathered at slightly cooler temperatures (15.9±3.7 °C). For a more appropriate comparison, the predictions of X_p for the corresponding temperatures were compared to measurements of X_p in Figure 4(b). Predictions were within ±50% of the measurements for more than 90% of the data. This fitting process assumed that the POA was in equilibrium. As we will show in Section 3.5, the POA may not have been in equilibrium for the lowest loadings in Figure 4, which may bias our fits in the lower volatility bins. We will discuss this bias in more detail in Section 3.4.

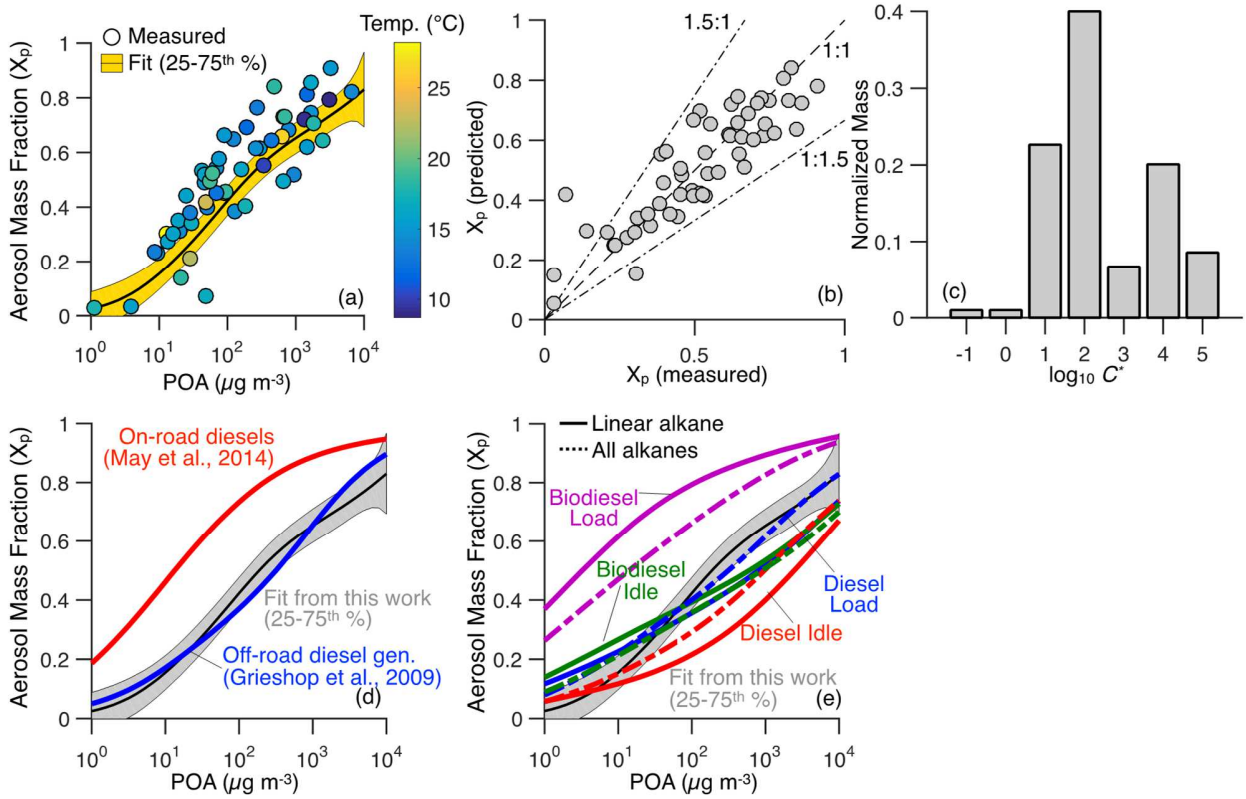

Figure 4: (a) Raw measurements of X_p-POA compared against predictions of X_p-POA based on the volatility-distribution fits; (b) Scatter plot comparing predictions of X_p based on the volatility-distribution fits against measurements; (c) Volatility distribution fit for the POA measured in this work; Predictions of X_p-POA based on the volatility-distribution fits compared against (d) those from earlier work and (e) those estimated through the distribution of alkanes .

The POA volatility from this study was compared to earlier work in Figure 4(d). Grieshop et al. (2009) used a thermal denuder in addition to isothermal dilution to estimate the gas/particle partitioning over a larger range of POA mass concentrations for POA from a small non-road diesel generator. May et al. (2013c) used four complementary methods – positive artifacts on quartz filters, dilution to an environmental chamber, heating with a thermal denuder, and POA speciation using TD-GC/MS – to estimate the POA from a suite of on-road medium- and heavy-duty diesel vehicles. The POA volatility from this work compared surprisingly well with the POA volatility determined by Grieshop et al. (2009) for the small non-road diesel generator. In contrast, the POA volatility in this work was much more volatile than that determined by May et al. (2013c) for on-road vehicles. We should note that the POA volatility measured by May et al. (2013c) was very similar to the POA volatility measured by Worton et al. (2014) from a roadway tunnel used by gasoline and diesel vehicles. This suggested that the on- and non-road vehicle POA volatility may be different, which could be attributed to the use of different fuels (i.e., on-road versus non-road diesel), differences in engine operation (i.e., steady state versus transient), and differences in the modes of contribution of the lubricating oil to the POA.

Finally, we compared the POA volatility from the volatility-distribution fits to the POA volatility predicted from the alkane-based volatility distributions that were developed from the TD-GC/MS

data (Figure 4(e)). The normalized volatility distributions from the TD-GC/MS data are tabulated in Table S2. The POA volatility predictions did not differ significantly between the linear alkane- and all alkane-based estimates from the TD-GC/MS results, suggesting that there were few systematic differences in the distribution of linear and other (i.e., branched and cyclic) alkanes with carbon number. Except for the predictions based on the biodiesel load volatility distributions, the POA volatility predictions based on the volatility distributions compared reasonably well between the two different approaches: positive artifact on quartz filters and alkane speciation using TD-GC/MS analysis. The only exception was that the alkane-based approach produced a slightly more volatile POA at POA values larger than 10-100 µg m^{-3} and a slightly less volatile POA at POA values smaller than 10 µg m^{-3}. It is unclear why the biodiesel load-based volatility distribution predicted a different POA volatility than the others and also did not agree with the volatility-distribution fits. For the Biodiesel-Load-None case, linear alkanes and total alkanes were 13% and 47% of the total OM respectively while for the other three cases (Diesel-Idle-None, Diesel-Load-None, and Biodiesel-Idle-None), linear alkanes and total alkanes were ~3% and ~29% of the total OM respectively. A larger fraction of the identified alkanes in the Biodiesel-Load-None case should have produced better agreement on the POA volatility between the volatility-distribution fits and the volatility distributions based on the TD-GC/MS data. We cannot explain this discrepancy.

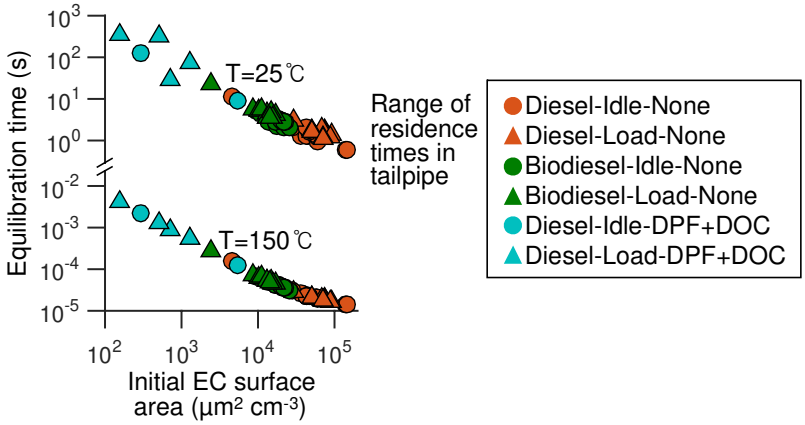

Figure 5: Model predicted equilibration times plotted against the initial EC surface area in the undiluted exhaust for all experiments performed in this work at two different temperatures: 150 and 25 ℃.

3.4 Kinetic Modeling

Sampling System. The kinetic model was first used to calculate the OM partitioning in the undiluted exhaust in the sampling system (i.e., stage 1, Figure 1) for all of the experiments performed in this work. The simulations were used to calculate the time required to achieve gas/particle equilibrium or the equilibration time, which was defined here as the time required for the particle mass to be within 99% of the final equilibrium value. The equilibration time is plotted in Figure 5 as a function of the initial seed surface area offered by the EC particles. The equilibration times were quite short at 150 °C and varied between 10^{-5} and 10^{-2} s. This was because the C^*s of the OM species at 150 °C were quite large (approximately seven orders of magnitude larger compared to those at 25 °C) and this required a very small amount of OM mass to be transferred to the particle phase. The equilibration time varied inversely with the initial EC

surface area, understandably because the higher initial EC surface area provided a larger condensational sink and a shorter timescale for condensation. Differences in the diesel and biodiesel experiments and the non-DPF+DOC and DPF+DOC experiments were hence expected since the use of biodiesel and a DPF+DOC resulted in lower EC emissions (see Figure 2). When compared to the range of residence times in the sampling system (0.3 to 3 s with an average ~1 s), the lower equilibration times meant that the POA had achieved gas/particle equilibrium in the sampling system. However, despite being in equilibrium, the high temperature meant that almost all of the OM mass was in the vapor phase with very little (<0.00002%) in the particle phase. A lot of this vapor mass is expected to condense in the dilution tunnel as the OM is cooled. The kinetics of this condensation are explored in the following paragraphs.

Dilution System. The kinetic model was used to calculate the OM partitioning after dilution (i.e., stage 2, Figure 1) for two different case studies. In the first case study, the POA partitioning was calculated as a function of the dilution ratio (1 to 10 or 1000) for a range of residence times (1, 10, 100, 310, and 1000 s) in the dilution tunnel for two representative experiments; the average residence time in the dilution tunnel in this work was ~310 s. The representative experiments we used were the Diesel-Load-None experiment (average tailpipe OM and EC mass concentrations of 8684 and 3485 $\mu g\ m^{-3}$ respectively) and Diesel-Load-DPF+DOC experiment (average tailpipe OM and EC mass concentrations of 159 and 28 $\mu g\ m^{-3}$ respectively) since the simulation results for these experiments seemed to capture the average behavior across the various fuel, engine-load, and emissions-control combinations. Based on findings from the previous section, the POA was assumed to be in equilibrium at the start of the simulation at the sampling system temperature of 150 °C (i.e., at the end of stage 1). We assumed that the dilution process was instantaneous and the diluted exhaust reached a temperature of 25 °C immediately. Results from these simulations are shown in Figure 6 (a) and (b). For reference, we also plot the change in the mass concentrations with dilution for a non-volatile POA.

POA mass concentrations at equilibrium were lower than those for the non-volatile case from evaporation of the semi-volatile fraction. For simulations performed at the different residence times for the Diesel-Load-None case, the POA mass concentrations agreed with the equilibrium values at lower dilution ratios but they deviated at higher dilution ratios when the equilibration times exceeded the residence times. The equilibration time (shown as a dotted black line) increased with the dilution ratio as the absolute particle mass concentrations and, proportionately, the condensational sinks were reduced. For instance, at a dilution ratio of 5 when the equilibration time was 10 s, a residence time of 10 s in the dilution tunnel was long enough that the POA mass concentration was nearly equal to the equilibrium value. In contrast, at a dilution ratio of 500 when the equilibration time was 1800 s, a residence time of 10 s in the dilution tunnel was too short to condense most of the POA and the POA mass concentration was only 13.7% of the equilibrium value. The same trends were observed for the Diesel-Load-DPF+DOC simulations with one key difference. As the initial (or undiluted) OM and EC concentrations were nearly two orders of magnitude lower with the emissions control (i.e., DPF+DOC), the equilibration times were relatively much longer, and the POA mass concentrations deviated from the equilibrium values even at very low dilution ratios. For instance, at a dilution ratio of 5 the equilibration time was 1800 s, and the POA mass concentrations at all residence times except for those at a 1000 s were substantially lower than those at equilibrium.

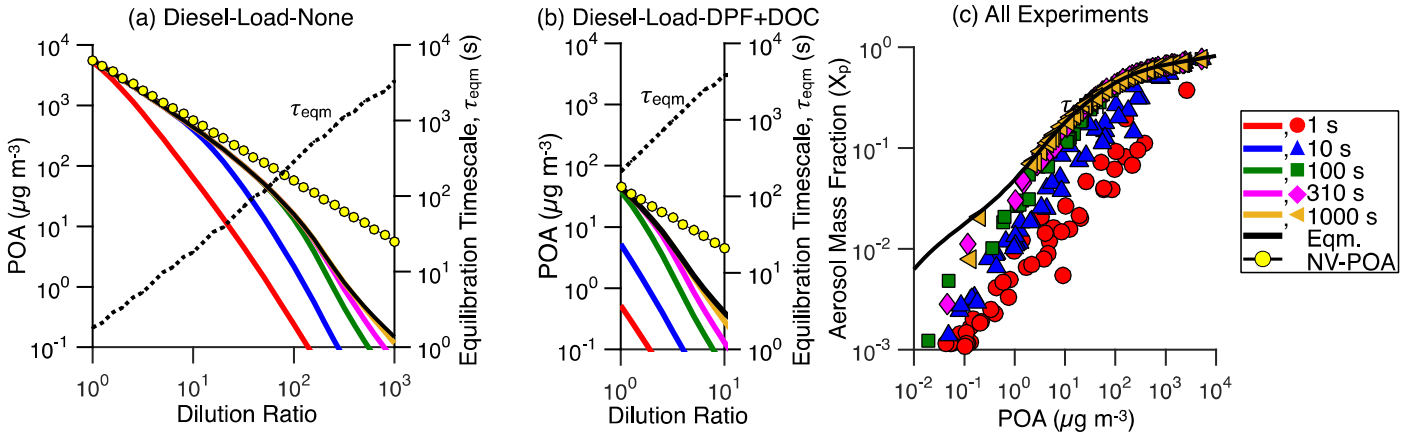

Figure 6: POA mass concentrations and equilibration times plotted against the dilution ratio for the average (a) Diesel-Load-None and (b) Diesel-Load-DPF+DOC experiment at different residence times in the dilution tunnel. (c) Aerosol mass fractions plotted against the POA mass concentrations for all experiments performed in this work at different residence times in the dilution tunnel.

The results in Figure 6 can be understood by considering the two competing effects at play when diluting hot exhaust: (1) cooling the exhaust reduces the C^*s of the OM species and promotes condensation of OM vapors versus (2) dilution-driven reduction in the absolute concentrations promotes evaporation of POA following Raoult's law. For both of the cases simulated in Figure 6(a) and (b), the simulations universally produced a POA mass concentration that was lower than the equilibrium value. This suggests that, given enough time, the OM vapors would continue to condense until they reached equilibrium and implies that the effects of cooling that promote condensation surpass the effects of dilution that promote evaporation. The simulation results further suggest that the POA mass concentrations in the dilution tunnel are sensitive to the undiluted particle concentration, dilution ratio, and residence time in the dilution tunnel. Commonly used dilution systems to measure particle emissions operate their systems at dilution ratios close to ten with residence times lower than ten seconds (40 CFR §1065, 2005). Based on the results presented in Figure 6(a), these dilution ratios and residence time inputs are likely to be sufficient for the POA to achieve equilibrium in the dilution tunnel for a diesel engine operated without an emissions control. However, these inputs to the dilution system would measure a substantially lower POA mass (factor of ~40) for diesel engines operated with an emissions control (Figure 6(b)). More broadly, we would expect the POA mass emissions to be similarly underestimated from modern combustion sources that are considerably cleaner than a diesel engine without an emissions controls (e.g., light-duty passenger vehicles, on-road trucks, gas turbines). Studies in the past have performed experiments at dilution ratios larger than ten to probe the POA volatility at atmospherically relevant concentrations (Lipsky and Robinson, 2006). Larger dilution ratios require longer equilibration times and our results suggest that residence times need to be increased proportionately to allow the POA to achieve equilibrium. A residence time of 1000 s produced near-perfect agreement with the equilibrium values up through a POA mass concentration of 1 μg m^{-3} for both the Diesel-Load-None and Diesel-Load-DPF+DOC simulations. Although long residence times might help achieve equilibrium, those on

651 the order of 1000 s or more might be impractical given the losses of vapors and particles to the
652 walls of the dilution tunnel.
653
654 In the second case study, the POA partitioning was calculated for all the experiments performed
655 in this work at experiment-specific dilution ratios but different residence times in the dilution
656 tunnel (1, 10, 100, 310, and 1000 s). Results from these simulations are shown in Figure 6(c).
657 Residence times of 1 and 10 s produced substantially lower aerosol mass fractions (X_p) when
658 compared to the equilibrium values for all POA loadings. At a C_{OA} of 10 µg m^{-3}, the X_p was a
659 factor of ~10 and ~3 lower than the equilibrium value for the 1 and 10 s simulations,
660 respectively. Short residence times, such as those found in conventional dilution systems (<10 s),
661 and particularly when diluting to atmospherically-relevant concentrations, are likely to
662 underestimate POA mass emissions. We should note that the BQ filters will still collect all of the
663 OM mass (i.e., vapors+POA) but will underestimate the POA mass emissions if these
664 measurements are artifact corrected based on the vapor mass collected on the QBT filters.
665 Further, data gathered at shorter residence times will point to a much more volatile POA than the
666 actual volatility. Longer residence times (≥100 s) produced better agreement of the X_ps with the
667 equilibrium values but eventually diverged at progressively lower POA values. For the residence
668 time used in this work (~310 s), the POA mass concentrations agreed well with the equilibrium
669 values up through a POA mass concentration of 10 µg m^{-3} and were approximately 30% lower
670 for POA mass concentrations between 1 and 10 µg m^{-3}. This partly validates the assumption in
671 Section 3.3 that the POA was in equilibrium before being sampled onto the filters for most of the
672 experiments performed in this work.
673
674 Although the equilibrium assumption was valid for most of the data, the volatility-distribution fit
675 may have underestimated the POA material in the lower-volatility bins (C^*<=1 µg m^{-3}) since
676 these were constrained to the measurements made at the lower POA mass concentrations
677 (POA<10 µg m^{-3}) where the POA did not condense fully towards equilibrium. With relatively
678 few data below 10 µg m^{-3}, we were unsuccessful in using the kinetic model to constrain the POA
679 mass in the lower-volatility bins. Furthermore, the volatility distributions based on the TD-
680 GC/MS data, shown in Figure 4(e), are consistent with there being more mass in the lower
681 volatility bins than in our volatility-distribution fit. Since the BQ filters collect all of the OM
682 mass (i.e., vapors+POA) and the TD-GC/MS analysis is performed on the total OM, the
683 calculated volatility distributions are independent of whether POA has achieved equilibrium
684 before being collected on the BQ filters. Hence, the TD-GC/MS-based technique offers promise
685 in constraining the distribution of POA mass in the lowest volatility bins. Having more mass in
686 the lowest-volatility bins, however, does not change the key findings from this work, i.e.,
687 residence times in the dilution tunnel need to be at least a few hundred seconds (or a few
688 minutes) to allow the POA to achieve equilibrium when measuring particle emissions from
689 cleaner, more modern sources and/or when diluting to atmospherically relevant concentrations.
690

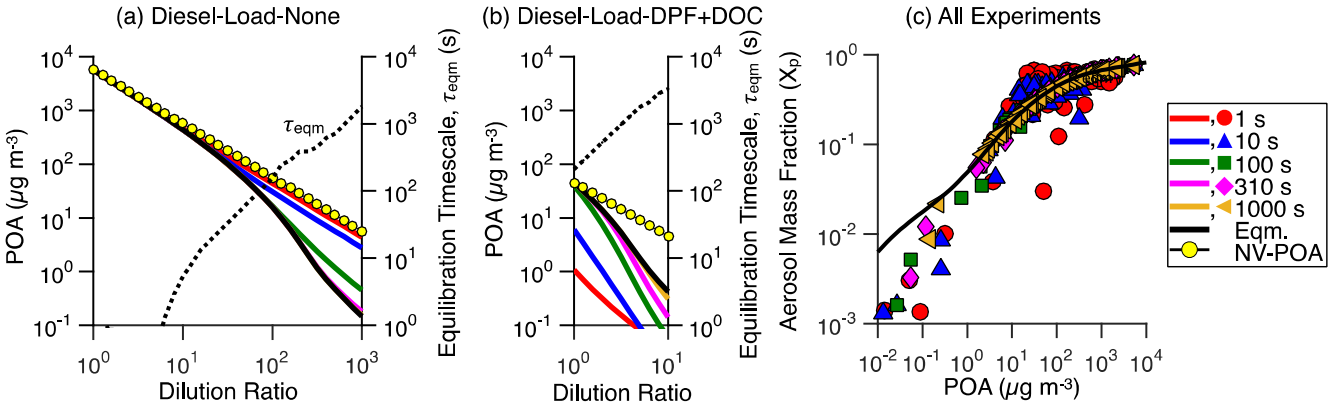

Figure 7: Same as Figure 6 but using an undiluted exhaust temperature of 25 °C.

The kinetics of gas/particle partitioning in the dilution tunnel were found to vary with the sampling temperature. Dilution setups may use sampling temperatures different than those used in this work. We used a higher sampling temperature in stage 1 of 150 °C to prevent condensation of water vapor and POA vapors onto the sampling tube walls. Serving as the other extreme, we simulated the equilibration times for undiluted POA at a typical laboratory temperature of 25 °C for stage 1. The equilibration times at 25 °C – shown in Figure 5 – were nearly five orders of magnitude larger than those at 150 °C and could be attributed to the large amounts of POA mass that needed to be transferred to the particle phase. If the undiluted exhaust in this work would have been cooled to 25 °C before dilution, POA would have achieved equilibrium in stage 1 in nearly three-quarters of the non-DPF+DOC experiments but not for any of the DPF+DOC experiments for the range of residence times in the sampling system. This has implications for the condensation/evaporation kinetics in the dilution tunnel, results for which are shown in Figure 7(a) for the Diesel-Load-None case and 7(b) for the Diesel-Load-DPF+DOC case respectively. For the Diesel-Load-None case, the POA was in equilibrium in the sampling system and dilution in the dilution tunnel resulted in evaporation of the POA mass. As there was no additional cooling, there was no driver for condensation. In contrast to the results shown in Figure 6(a), shorter residence times at higher dilution ratios (>10) produced a higher POA mass concentration than the equilibrium value because the residence times were too short to allow the POA to evaporate. It was interesting to note that the simulated POA mass concentrations for the shortest residence time of 1 s were similar to those for non-volatile POA. The POA was not in equilibrium in the sampling system for the Diesel-Load-DPF+DOC case with an abundance of condensable mass in the vapor phase. Similar to the trends shown in Figure 6(b), shorter residence times produced POA mass concentrations lower than the equilibrium values and increasing the residence times allowed the POA to condense until it reached equilibrium. This result suggests that the use of lower sampling temperatures would still result in an underestimation of POA mass concentrations at shorter residence times for cleaner, more modern sources. When examining the response to the residence times for all the experiments performed in this work (Figure 7(c)), lower residence times (≤10 s) produced a higher X_p than the equilibrium value for most of the experiments but produced a lower X_p than the equilibrium value at lower POA mass concentrations. These simulations at the lower sampling temperature indicate that insufficient residence times in the dilution tunnel may bias the POA mass emissions

lower or higher, where the direction of the bias – all things being equal – will depend on whether the POA has achieved equilibrium in the sampling system.

4. Summary and Conclusions

Our work makes four key contributions to understanding the POA volatility from diesel engines: (i) POA volatility is independent of fuel, engine load, or emissions control, (ii) POA volatility is different between on- and non-road diesel engines, (iii) speciation of alkanes in diesel POA can be used to infer its volatility and particularly that of its least volatile components, and (iv) dilution systems need to use longer residence times to allow POA to achieve gas/particle equilibrium before being sampled and/or measured, especially for cleaner, modern combustion sources. A summary of those contributions and their implications for measuring and modeling the volatility of POA are discussed below.

POA from a modern-day non-road diesel engine was found to be semi-volatile in agreement with previous work (May et al., 2013c; Robinson et al., 2007). But surprisingly, the gas/particle partitioning did not appear to be very sensitive to the choice of fuel, engine load, or emissions control. Although not specific to fuel or engine load, May et al. (2013c) made a similar conclusion about POA volatility from on-road diesel vehicles equipped with varying emissions controls and operated on different drive cycles. This observation might offer advantages in modeling POA emissions in atmospheric models as the same volatility distribution could be used to represent POA from diesel-powered sources operated with different fuels, engine loads, and emissions control configurations. Our results suggest that at ambient temperatures (298 K), ~80% of the tailpipe POA mass is likely to evaporate with dilution to atmospherically relevant concentrations (5-10 $\mu g\ m^{-3}$). This dilution is likely to happen rapidly on time scales of minutes and spatial scales of 100s of meters. Since POA is expected to dominate the $PM_{2.5}$ emissions (~60-90%) from modern diesel sources (May et al., 2014), evaporation of POA with dilution will significantly affect the contribution of diesel sources to mass concentrations and properties of ambient $PM_{2.5}$. Hence, it is important that POA from diesel engines is treated as semi-volatile in atmospheric models.

The POA volatility measured in this work for a more representative non-road diesel engine agreed quite well with that estimated for a relatively less representative non-road engine studied more than a decade ago (Grieshop et al., 2009; Robinson et al., 2007). To our knowledge, these two engines are the only non-road engines that have been studied to characterize POA volatility. However, both engines produced a much more volatile POA than that produced by a suite of on-road engines (May et al., 2013c). For example, at an ambient OA mass concentration of 10 $\mu g\ m^{-3}$, ~80% of the non-road POA emissions are expected to evaporate based on this work while only about half of the on-road POA emissions are expected to do so based on the work of May et al. (2013c). This finding has implications for the contribution of on- and non-road diesel-powered sources to ambient POA and $PM_{2.5}$, as well as the atmospheric production of secondary organic aerosol as the evaporated POA vapors can oxidize to form condensable products (Miracolo et al., 2010). As the POA volatility is different, POA may need to be treated uniquely for on- and non-road sources in atmospheric models.

Linear and branched/cyclic alkanes in the POA were speciated and mapped in volatility space to estimate a volatility distribution for POA. As has been shown in prior work (May et al., 2013b,c;

Presto et al., 2011), this volatility distribution was able to reasonably predict the observed gas/particle partitioning of POA, implying that speciation of POA can be used as an alternative approach to quantifying and modeling the POA volatility (May et al., 2013b,c; Presto et al., 2011). In particular, this technique offers promise in constraining the distribution of the POA mass in the lowest volatility bins because it does not require the POA to have achieved equilibrium with its vapors when it is being sampled. Recently, a suite of novel instrumentation and techniques has enabled detailed speciation of organic compounds present in gas and particle phase emissions of combustion sources (Gentner et al., 2012; Koss et al., 2018; May et al., 2014; Worton et al., 2014). These new resources will enable better and more complete speciation and consequently improve estimates of POA volatility without the need to perform filter measurements across a range of dilution ratios as done in this work.

The kinetic modeling performed in this work suggests that residence times in the dilution tunnel need to be on the order of minutes to allow the POA in the diluted exhaust to achieve gas/particle equilibrium. This finding is especially true in the case of particle measurements from cleaner, more modern sources that produce very few particle emissions and/or those that have been significantly diluted. To highlight the significance of this finding for real-world sampling, we used the kinetic model to simulate POA partitioning in the dilution tunnel across a range of tailpipe concentrations and residence times in the dilution tunnel. We varied the tailpipe EC (or seed) mass concentrations between 0.5 and 50,000 µg m^{-3} to roughly capture the emission factor range observed for EC over the diesel engine/vehicle fleet; from 100-1000 mg kg-$fuel^{-1}$ for non-DPF diesels to 0.05-1 mg kg-$fuel^{-1}$ for non-DPF diesels (May et al., 2014). We assumed an OC:EC mass ratio of 3 but changing the ratio between 0.5 to 10 did not change the findings significantly. The residence time was varied between 1 and 10,000 s, understanding that residence times in conventional dilution systems are much shorter than a minute. The dilution ratio was held constant at 10 to match the average dilution ratio used in conventional dilution systems. Simulations were performed separately for an undiluted exhaust temperature of 150 and 25 °C.

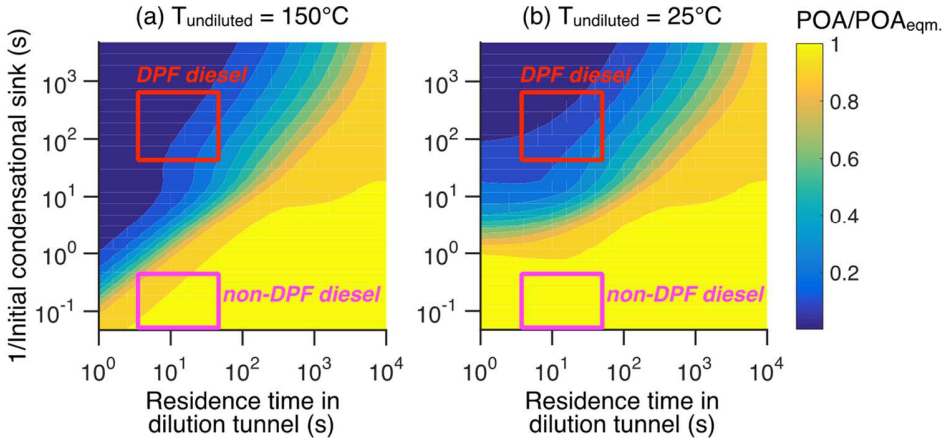

Figure 8: Ratio of predicted POA mass concentration to the equilibrium POA value over a range of initial condensational sinks and residence times in the dilution tunnel for undiluted exhaust at (a) 150 °C and (b) 25 °C.

Results, plotted in Figure 8, show that the POA mass concentration was close to its equilibrium value or that the POA had achieved gas/particle equilibrium when the initial condensational sink was high (or the inverse was low) and/or the residence time in the dilution tunnel was long. As a result, for short initial condensational-sink timescales there should be very little bias (small bias in the 150 °C simulations but even smaller bias in the 25 °C simulations) in the POA mass emissions measured from non-DPF diesels. In contrast, for the DPF cases with long initial condensation-sink timescales, the POA mass concentrations were only between 5 to 20% of the equilibrium values, and POA mass emissions measured from DPF diesels could be significantly underestimated. If the POA mass is being measured using quartz filters, the POA mass emissions will only be underestimated if the measurements are artifact corrected for vapor mass collected on backup quartz filters. Direct-reading instruments, on the other hand, will always underestimate the POA mass emissions. For diesel engines equipped with DPFs and similar cleaner, more modern sources, we recommend the use of long residence times (few minutes) in dilution tunnels to allow the POA to achieve equilibrium before it is sampled. In cases where the residence times cannot be changed, we recommend that kinetic models, similar to those used in this work or to interpret thermal denuder data, be used to interpret measurements.

One of the shortcomings of our model is that we did not consider the influence of nucleation on our findings. Prior research has shown that sudden cooling of the hot exhaust in the dilution tunnel under the right, input (e.g., high sulfur content), operating (e.g., high relative humidity) and engine conditions (e.g., idle loads) will result in new particle formation or nucleation (Harrison et al., 2018). These freshly nucleated particles will continue to grow from condensation of OM vapors and could substantially increase the condensational sink and shorten the equilibration times. If nucleation is commonly observed in dilution tunnels, for which there are very little data, it would weaken our primary finding that longer residence times be required in dilution tunnels to allow the POA to achieve equilibrium prior to measurement. We also did not model coagulation of particles in this work. Coagulation is expected to be active only at lower dilution ratios when the number concentrations are high enough ($>10^6$ cm^{-3} at a residence time of 1000 s (Hinds, 1999)). Since the condensational sinks at lower dilution ratios are large enough to keep the equilibration times short (see Figures 6(a) and 7(a)), any coagulation to reduce the condensational sink will have a negligible influence, compared to that of condensation, on the equilibration times.

5. Acknowledgements

SHJ acknowledges support from the Ralph E. Powe Junior Faculty Enhancement Award and the National Oceanic and Atmospheric Administration (NA17OAR4310003). We would like to thank the staff at the Engines and Energy Conversion Laboratory (Liam Lewane, Mark James, and Kirk Evans) for facilitating and conducting the engine experiments. We would also like to thank Drs. Sulekha Chattopadhyay, Reddy Yatavelli, Andrew May, Daniel Olsen, and Todd Bandhauer for useful discussions.

6. References

Abdul-Khalek, I.S., Kittelson, D.B., 1995. Real Time Measurement of Volatile and Solid Exhaust Particles Using a Catalytic Stripper. SAE Trans. J. Mater. Manuf. 104, 462–478.

Aiken, A.C., DeCarlo, P.F., Kroll, J.H., Worsnop, D.R., Huffman, J.A., Docherty, K.S., Ulbrich, I.M., Mohr, C., Kimmel, J.R., Sueper, D., Sun, Y., Zhang, Q., Trimborn, A., Northway, M.,

852 Ziemann, P.J., Canagaratna, M.R., Onasch, T.B., Alfarra, M.R., Prevot, A.S.H., Dommen,
853 J., Duplissy, J., Metzger, A., Baltensperger, U., Jimenez, J.L., 2008. O/C and OM/OC
854 Ratios of Primary, Secondary, and Ambient Organic Aerosols with High-Resolution Time-
855 of-Flight Aerosol Mass Spectrometry. Environ. Sci. Technol. 42, 4478–4485.
856 Anenberg, S., Miller, J., Henze, D., Minjares, R., 2019. A global snapshot of the air pollution-
857 related health impacts of transportation sector emissions in 2010 and 2015. International
858 Council on Clean Transportation: Washington, DC, USA.
859 Biswas, S., Verma, V., Schauer, J.J., Cassee, F.R., Cho, A.K., Sioutas, C., 2009. Oxidative
860 Potential of Semi-Volatile and Non Volatile Particulate Matter (PM) from Heavy-Duty
861 Vehicles Retrofitted with Emission Control Technologies. Environ. Sci. Technol. 43, 3905–
862 3912.
863 Cavalli, F., Viana, M., Yttri, K.E., Genberg, J., Putaud, J.-P., 2010. Toward a standardised
864 thermal-optical protocol for measuring atmospheric organic and elemental carbon: the
865 EUSAAR protocol. Atmospheric Measurement Techniques 3, 79–89.
866 Cheung, K.L., Ntziachristos, L., Tzamkiozis, T., Schauer, J.J., Samaras, Z., Moore, K.F., Sioutas,
867 C., 2010. Emissions of Particulate Trace Elements, Metals and Organic Species from
868 Gasoline, Diesel, and Biodiesel Passenger Vehicles and Their Relation to Oxidative
869 Potential. Aerosol Sci. Technol. 44, 500–513.
870 Chow, J.C., Watson, J.G., Chen, L.W.A., Arnott, W.P., Moosmüller, H., Fung, K., 2004.
871 Equivalence of elemental carbon by thermal/optical reflectance and transmittance with
872 different temperature protocols. Environ. Sci. Technol. 38, 4414–4422.
873 Dallmann, T.R., Harley, R.A., 2010. Evaluation of mobile source emission trends in the United
874 States. J. Geophys. Res. 115, 1033.
875 Donahue, N.M., Robinson, A.L., Stanier, C.O., Pandis, S.N., 2006. Coupled partitioning,
876 dilution, and chemical aging of semivolatile organics. Environ. Sci. Technol. 40, 2635–
877 2643.
878 Drenth, A.C., Olsen, D.B., Cabot, P.E., Johnson, J.J., 2014. Compression ignition engine
879 performance and emission evaluation of industrial oilseed biofuel feedstocks camelina,
880 carinata, and pennycress across three fuel pathways. Fuel 136, 143–155.
881 Eller, P.M., Cassinelli, M.E., 1996. Niosh, Elemental Carbon (Diesel Particulate): Method 5040.
882 NIOSH Manual of Analytical Methods. National Institute for Occupational Safety and
883 Health: Cincinatti, OH, USA 2003–2154.
884 Fuzzi, S., Baltensperger, U., Carslaw, K., Decesari, S., Denier van der Gon, H., Facchini, M.C.,
885 Fowler, D., Koren, I., Langford, B., Lohmann, U., Nemitz, E., Pandis, S., Riipinen, I.,
886 Rudich, Y., Schaap, M., Slowik, J.G., Spracklen, D.V., Vignati, E., Wild, M., Williams, M.,
887 Gilardoni, S., 2015. Particulate matter, air quality and climate: lessons learned and future
888 needs. Atmos. Chem. Phys. 15, 8217–8299.
889 Gentner, D.R., Isaacman, G., Worton, D.R., Chan, A.W.H., Dallmann, T.R., Davis, L., Liu, S.,
890 Day, D.A., Russell, L.M., Wilson, K.R., Weber, R., Guha, A., Harley, R.A., Goldstein,
891 A.H., 2012. Elucidating secondary organic aerosol from diesel and gasoline vehicles
892 through detailed characterization of organic carbon emissions. Proc. Natl. Acad. Sci. U. S.
893 A. 109, 18318–18323.
894 Gordon, T.D., Presto, A.A., Nguyen, N.T., Robertson, W.H., Na, K., Sahay, K.N., Zhang, M.,
895 Maddox, C., Rieger, P., Chattopadhyay, S., Maldonado, H., Maricq, M.M., Robinson, A.L.,
896 2014. Secondary organic aerosol production from diesel vehicle exhaust: impact of
897 aftertreatment, fuel chemistry and driving cycle. Atmospheric Chemistry & Physics 14,

898 4643–4659.
899 Grieshop, A.P., Logue, J.M., Donahue, N.M., 2009. Laboratory investigation of photochemical
900 oxidation of organic aerosol from wood fires 1: measurement and simulation of organic
901 aerosol evolution. Atmospheric.
902 Guan, C., Cheung, C.S., Li, X., Li, D., Huang, Z., 2017. Effects of engine load and dilution
903 conditions on gas-particle partitioning of primary organic aerosol emitted from a light-duty
904 diesel engine. J. Aerosol Sci. 104, 32–42.
905 Harrison Roy M., Rob MacKenzie A., Xu Hongming, Alam Mohammed S., Nikolova Irina,
906 Zhong Jian, Singh Ajit, Zeraati-Rezaei Soheil, Stark Christopher, Beddows David C. S.,
907 Liang Zhirong, Xu Ruixin, Cai Xiaoming, 2018. Diesel exhaust nanoparticles and their
908 behaviour in the atmosphere. Proceedings of the Royal Society A: Mathematical, Physical
909 and Engineering Sciences 474, 20180492.
910 Hildemann, L.M., Cass, G.R., Markowski, G.R., 1989. A Dilution Stack Sampler for Collection
911 of Organic Aerosol Emissions: Design, Characterization and Field Tests. Aerosol Sci.
912 Technol. 10, 193–204.
913 Huffman, J.A., Docherty, K.S., Mohr, C., Cubison, M.J., Ulbrich, I.M., Ziemann, P.J., Onasch,
914 T.B., Jimenez, J.L., 2009. Chemically-resolved volatility measurements of organic aerosol
915 fom different sources. Environ. Sci. Technol. 43, 5351–5357.
916 Jathar, S.H., Friedman, B., Galang, A.A., Link, M.F., Brophy, P., Volckens, J., Eluri, S., Farmer,
917 D.K., 2017. Linking Load, Fuel, and Emission Controls to Photochemical Production of
918 Secondary Organic Aerosol from a Diesel Engine. Environ. Sci. Technol. 51, 1377–1386.
919 Kim, Y., Sartelet, K., Seigneur, C., Charron, A., Besombes, J.-L., Jaffrezo, J.-L., Marchand, N.,
920 Polo, L., 2016. Effect of measurement protocol on organic aerosol measurements of exhaust
921 emissions from gasoline and diesel vehicles. Atmos. Environ. 140, 176–187.
922 Ko, J., Myung, C.-L., Park, S., 2019. Impacts of ambient temperature, DPF regeneration, and
923 traffic congestion on NOx emissions from a Euro 6-compliant diesel vehicle equipped with
924 an LNT under real-world driving conditions. Atmos. Environ. 200, 1–14.
925 Koss, A.R., Sekimoto, K., Gilman, J.B., Selimovic, V., Coggon, M.M., Zarzana, K.J., Yuan, B.,
926 Lerner, B.M., Brown, S.S., Jimenez, J.L., Krechmer, J., Roberts, J.M., Warneke, C.,
927 Yokelson, R.J., Gouw, J. de, 2018. Non-methane organic gas emissions from biomass
928 burning: identification, quantification, and emission factors from PTR-ToF during the
929 FIREX 2016 laboratory experiment. Atmos. Chem. Phys. 18, 3299–3319.
930 Kuwayama, T., Collier, S., Forestieri, S., Brady, J.M., Bertram, T.H., Cappa, C.D., Zhang, Q.,
931 Kleeman, M.J., 2015. Volatility of primary organic aerosol emitted from light duty gasoline
932 vehicles. Environ. Sci. Technol. 49, 1569–1577.
933 Lack, D.A., Lovejoy, E.R., Baynard, T., Pettersson, A., Ravishankara, A.R., 2006. Aerosol
934 Absorption Measurement using Photoacoustic Spectroscopy: Sensitivity, Calibration, and
935 Uncertainty Developments. Aerosol Sci. Technol. 40, 697–708.
936 Lipsky, E.M., Robinson, A.L., 2006. Effects of Dilution on Fine Particle Mass and Partitioning
937 of Semivolatile Organics in Diesel Exhaust and Wood Smoke. Environ. Sci. Technol. 40,
938 155–162.
939 Li, X., Dallmann, T.R., May, A.A., Tkacik, D.S., Lambe, A.T., Jayne, J.T., Croteau, P.L., Presto,
940 A.A., 2016. Gas-Particle Partitioning of Vehicle Emitted Primary Organic Aerosol
941 Measured in a Traffic Tunnel. Environ. Sci. Technol. 50, 12146–12155.
942 Lopez-Hilfiker, F.D., Iyer, S., Mohr, C., Lee, B.H., 2016. Constraining the sensitivity of iodide
943 adduct chemical ionization mass spectrometry to multifunctional organic molecules using

944 the collision limit and thermodynamic …. Atmospheric.
945 Lopez-Hilfiker, F.D., Mohr, C., Ehn, M., Rubach, F., Kleist, E., Wildt, J., Mentel, T.F., Lutz, A.,
946 Hallquist, M., Worsnop, D., Thornton, J.A., 2014. A novel method for online analysis of
947 gas and particle composition: description and evaluation of a Filter Inlet for Gases and
948 AEROsols (FIGAERO). Atmospheric Measurement Techniques 7, 983–1001.
949 May, A.A., Levin, E.J.T., Hennigan, C.J., Riipinen, I., Lee, T., Collett, J.L., Jr., Jimenez, J.L.,
950 Kreidenweis, S.M., Robinson, A.L., 2013a. Gas-particle partitioning of primary organic
951 aerosol emissions: 3. Biomass burning. J. Geophys. Res. D: Atmos. 118, 11,327–11,338.
952 May, A.A., Nguyen, N.T., Presto, A.A., Gordon, T.D., Lipsky, E.M., Karve, M., Gutierrez, A.,
953 Robertson, W.H., Zhang, M., Brandow, C., Chang, O., Chen, S., Cicero-Fernandez, P.,
954 Dinkins, L., Fuentes, M., Huang, S.-M., Ling, R., Long, J., Maddox, C., Massetti, J.,
955 McCauley, E., Miguel, A., Na, K., Ong, R., Pang, Y., Rieger, P., Sax, T., Truong, T., Vo,
956 T., Chattopadhyay, S., Maldonado, H., Maricq, M.M., Robinson, A.L., 2014. Gas- and
957 particle-phase primary emissions from in-use, on-road gasoline and diesel vehicles. Atmos.
958 Environ. 88, 247–260.
959 May, A.A., Presto, A.A., Hennigan, C.J., Nguyen, N.T., Gordon, T.D., Robinson, A.L., 2013b.
960 Gas-particle partitioning of primary organic aerosol emissions: (1) Gasoline vehicle
961 exhaust. Atmos. Environ. 77, 128–139.
962 May, A.A., Presto, A.A., Hennigan, C.J., Nguyen, N.T., Gordon, T.D., Robinson, A.L., 2013c.
963 Gas-particle partitioning of primary organic aerosol emissions: (2) diesel vehicles. Environ.
964 Sci. Technol. 47, 8288–8296.
965 Miracolo, M.A., Presto, A.A., Lambe, A.T., Hennigan, C.J., Donahue, N.M., Kroll, J.H.,
966 Worsnop, D.R., Robinson, A.L., 2010. Photo-oxidation of low-volatility organics found in
967 motor vehicle emissions: production and chemical evolution of organic aerosol mass.
968 Environ. Sci. Technol. 44, 1638–1643.
969 Mohr, C., Huffman, J.A., Cubison, M.J., Aiken, A.C., Docherty, K.S., Kimmel, J.R., Ulbrich,
970 I.M., Hannigan, M., Jimenez, J.L., 2009. Characterization of primary organic aerosol
971 emissions from meat cooking, trash burning, and motor vehicles with high-resolution
972 aerosol mass spectrometry and comparison with ambient and chamber observations.
973 Environ. Sci. Technol. 43, 2443–2449.
974 Ning, Z., Chan, K.L., Wong, K.C., Westerdahl, D., Močnik, G., Zhou, J.H., Cheung, C.S., 2013.
975 Black carbon mass size distributions of diesel exhaust and urban aerosols measured using
976 differential mobility analyzer in tandem with Aethalometer. Atmos. Environ. 80, 31–40.
977 Oliveira, L. S., Franca, A. S., Camargos, R. R. S., and Ferraz, V. P., 2008. Coffee oil as a
978 potential feedstock for biodiesel production, Bioresource Technology, 99, 3244-3250.
979 Pachauri, R.K., Allen, M.R., Barros, V.R., Broome, J., Cramer, W., Christ, R., Church, J.A.,
980 Clarke, L., Dahe, Q., Dasgupta, P., Dubash, N.K., Edenhofer, O., Elgizouli, I., Field, C.B.,
981 Forster, P., Friedlingstein, P., Fuglestvedt, J., Gomez-Echeverri, L., Hallegatte, S., Hegerl,
982 G., Howden, M., Jiang, K., Jimenez Cisneroz, B., Kattsov, V., Lee, H., Mach, K.J.,
983 Marotzke, J., Mastrandrea, M.D., Meyer, L., Minx, J., Mulugetta, Y., O'Brien, K.,
984 Oppenheimer, M., Pereira, J.J., Pichs-Madruga, R., Plattner, G.-K., Pörtner, H.-O., Power,
985 S.B., Preston, B., Ravindranath, N.H., Reisinger, A., Riahi, K., Rusticucci, M., Scholes, R.,
986 Seyboth, K., Sokona, Y., Stavins, R., Stocker, T.F., Tschakert, P., van Vuuren, D., van
987 Ypserle, J.-P., 2014. Climate Change 2014: Synthesis Report. Contribution of Working
988 Groups I, II and III to the Fifth Assessment Report of the Intergovernmental Panel on
989 Climate Change. IPCC, Geneva, Switzerland.

990 Pankow, J.F., Asher, W.E., 2008. SIMPOL.1: a simple group contribution method for predicting
991 vapor pressures and enthalpies of vaporization of multifunctional organic compounds.
992 Atmos. Chem. Phys. 8, 2773–2796.
993 Pauls, R. E., 2011. A Review of Chromatographic Characterization Techniques for Biodiesel and
994 Biodiesel Blends, Journal of Chromatographic Science, 49, 384-396.
995 Pope, C.A., III, Burnett, R.T., Krewski, D., Jerrett, M., Shi, Y., Calle, E.E., Thun, M.J., 2009.
996 CLINICAL PERSPECTIVE. Circulation 120, 941–948.
997 Presto, A.A., Hennigan, C.J., Nguyen, N.T., Robinson, A.L., 2012. Determination of volatility
998 distributions of primary organic aerosol emissions from internal combustion engines using
999 thermal desorption gas chromatography mass spectrometry. Aerosol Sci. Technol. 46,
1000 1129–1139.
1001 Presto, A.A., Miracolo, M.A., Donahue, N.M., Robinson, A.L., 2010. Secondary organic aerosol
1002 formation from high-NO(x) photo-oxidation of low volatility precursors: n-alkanes.
1003 Environ. Sci. Technol. 44, 2029–2034.
1004 Presto, A.A., Nguyen, N.T., Ranjan, M., Reeder, A.J., Lipsky, E.M., Hennigan, C.J., Miracolo,
1005 M.A., Riemer, D.D., Robinson, A.L., 2011. Fine particle and organic vapor emissions from
1006 staged tests of an in-use aircraft engine. Atmos. Environ. 45, 3603–3612.
1007 Ranjan, M., Presto, A.A., May, A.A., Robinson, A.L., 2012. Temperature Dependence of Gas–
1008 Particle Partitioning of Primary Organic Aerosol Emissions from a Small Diesel Engine.
1009 Aerosol Sci. Technol. 46, 13–21.
1010 Riipinen, I., Pierce, J.R., Donahue, N.M., Pandis, S.N., 2010. Equilibration time scales of
1011 organic aerosol inside thermodenuders: Evaporation kinetics versus thermodynamics.
1012 Atmos. Environ. 44, 597–607.
1013 Robinson, A.L., Donahue, N.M., Shrivastava, M.K., Weitkamp, E.A., Sage, A.M., Grieshop,
1014 A.P., Lane, T.E., Pierce, J.R., Pandis, S.N., 2007. Rethinking organic aerosols: semivolatile
1015 emissions and photochemical aging. Science 315, 1259–1262.
1016 Saliba, G., Saleh, R., Zhao, Y., Presto, A.A., Lambe, A.T., Frodin, B., Sardar, S., Maldonado, H.,
1017 Maddox, C., May, A.A., Drozd, G.T., Goldstein, A.H., Russell, L.M., Hagen, F., Robinson,
1018 A.L., 2017. Comparison of Gasoline Direct-Injection (GDI) and Port Fuel Injection (PFI)
1019 Vehicle Emissions: Emission Certification Standards, Cold-Start, Secondary Organic
1020 Aerosol Formation Potential, and Potential Climate Impacts. Environ. Sci. Technol. 51,
1021 6542–6552.
1022 Schauer, J.J., Fraser, M.P., Cass, G.R., Simoneit, B.R.T., 2002. Source reconciliation of
1023 atmospheric gas-phase and particle-phase pollutants during a severe photochemical smog
1024 episode. Environ. Sci. Technol. 36, 3806–3814.
1025 Schauer, J.J., Kleeman, M.J., Cass, G.R., 1999. Measurement of Emissions from Air Pollution
1026 Sources. 2. C1 through C30 Organic Compounds from Medium Duty Diesel Trucks. Sci.
1027 Technol. China.
1028 Schill, G.P., Jathar, S.H., Kodros, J.K., Levin, E.J.T., Galang, A.M., Friedman, B., Link, M.F.,
1029 Farmer, D.K., Pierce, J.R., Kreidenweis, S.M., DeMott, P.J., 2016. Ice-nucleating particle
1030 emissions from photochemically aged diesel and biodiesel exhaust: Diesel Exhaust Ice-
1031 Nucleating Particles. Geophys. Res. Lett. 43, 5524–5531.
1032 Sharma, N., Vanderheyden, C., Klunder, K., Henry, C.S., Volckens, J., Jathar, S.H., 2019.
1033 Emerging investigator series: oxidative potential of diesel exhaust particles: role of fuel,
1034 engine load, and emissions control. Environ. Sci. Process. Impacts 21, 819–830.
1035 Shi, J.P., Harrison, R.M., 1999. Investigation of Ultrafine Particle Formation during Diesel

Exhaust Dilution. Environ. Sci. Technol. 33, 3730–3736.
Shrivastava, M.K., Lipsky, E.M., Stanier, C.O., Robinson, A.L., 2006. Modeling Semivolatile Organic Aerosol Mass Emissions from Combustion Systems. Environ. Sci. Technol. 40, 2671–2677.
Stark, H., Yatavelli, R.L.N., Thompson, S.L., Kang, H., Krechmer, J.E., Kimmel, J.R., Palm, B.B., Hu, W., Hayes, P.L., Day, D.A., Campuzano-Jost, P., Canagaratna, M.R., Jayne, J.T., Worsnop, D.R., Jimenez, J.L., 2017. Impact of Thermal Decomposition on Thermal Desorption Instruments: Advantage of Thermogram Analysis for Quantifying Volatility Distributions of Organic Species. Environ. Sci. Technol. 51, 8491–8500.
Subramanian, R., Khlystov, A.Y., Cabada, J.C., Robinson, A.L., 2004. Positive and Negative Artifacts in Particulate Organic Carbon Measurements with Denuded and Undenuded Sampler Configurations Special Issue of Aerosol Science and Technology on Findings from the Fine Particulate Matter Supersites Program. Aerosol Sci. Technol. 38, 27–48.
Sumiya, S., Oyamada, H., Fujita, T., Nakamura, K., Osumi, K., Tashiro, Y., 2009. Highly robust diesel oxidation catalyst for dual mode combustion system. SAE Technical Paper.
Tröstl, J., Chuang, W.K., Gordon, H., Heinritzi, M., Yan, C., Molteni, U., Ahlm, L., Frege, C., Bianchi, F., Wagner, R., Simon, M., Lehtipalo, K., Williamson, C., Craven, J.S., Duplissy, J., Adamov, A., Almeida, J., Bernhammer, A.-K., Breitenlechner, M., Brilke, S., Dias, A., Ehrhart, S., Flagan, R.C., Franchin, A., Fuchs, C., Guida, R., Gysel, M., Hansel, A., Hoyle, C.R., Jokinen, T., Junninen, H., Kangasluoma, J., Keskinen, H., Kim, J., Krapf, M., Kürten, A., Laaksonen, A., Lawler, M., Leiminger, M., Mathot, S., Möhler, O., Nieminen, T., Onnela, A., Petäjä, T., Piel, F.M., Miettinen, P., Rissanen, M.P., Rondo, L., Sarnela, N., Schobesberger, S., Sengupta, K., Sipilä, M., Smith, J.N., Steiner, G., Tomè, A., Virtanen, A., Wagner, A.C., Weingartner, E., Wimmer, D., Winkler, P.M., Ye, P., Carslaw, K.S., Curtius, J., Dommen, J., Kirkby, J., Kulmala, M., Riipinen, I., Worsnop, D.R., Donahue, N.M., Baltensperger, U., 2016. The role of low-volatility organic compounds in initial particle growth in the atmosphere. Nature 533, 527–531.
Turpin, B.J., Lim, H.-J., 2001. Species Contributions to PM2.5 Mass Concentrations: Revisiting Common Assumptions for Estimating Organic Mass. Aerosol Sci. Technol. 35, 602–610.
Worton, D.R., Isaacman, G., Gentner, D.R., Dallmann, T.R., Chan, A.W.H., Ruehl, C., Kirchstetter, T.W., Wilson, K.R., Harley, R.A., Goldstein, A.H., 2014. Lubricating oil dominates primary organic aerosol emissions from motor vehicles. Environ. Sci. Technol. 48, 3698–3706.
Zhang, Y., Zhang, Q., Cheng, Y., Su, H., Kecorius, S., Wang, Z., Wu, Z., Hu, M., Zhu, T., Wiedensohler, A., He, K., 2016. Measuring the morphology and density of internally mixed black carbon with SP2 and VTDMA: new insight into the absorption enhancement of black carbon in the atmosphere. Atmospheric Measurement Techniques 9, 1833–1843.
Zhao, Y., Hennigan, C.J., May, A.A., Tkacik, D.S., de Gouw, J.A., Gilman, J.B., Kuster, W.C., Borbon, A., Robinson, A.L., 2014. Intermediate-Volatility Organic Compounds: A Large Source of Secondary Organic Aerosol. Environ. Sci. Technol. 48, 13743–13750.
Zhao, Y., Nguyen, N.T., Presto, A.A., Hennigan, C.J., May, A.A., Robinson, A.L., 2016. Intermediate Volatility Organic Compound Emissions from On-Road Gasoline Vehicles and Small Off-Road Gasoline Engines. Environ. Sci. Technol. 50, 4554–4563.
Zhao, Y., Nguyen, N.T., Presto, A.A., Hennigan, C.J., May, A.A., Robinson, A.L., 2015. Intermediate Volatility Organic Compound Emissions from On-Road Diesel Vehicles: Chemical Composition, Emission Factors, and Estimated Secondary Organic Aerosol

1082 Production. Environ. Sci. Technol. 49, 11516–11526.